GAN-Control: Explicitly Controllable GANs

Alon Shoshan
Amazon One
alonshos@amazon.com

Nadav Bhonker
Amazon One
nadavb@amazon.com

Igor Kviatkovsky
Amazon One
kviat@amazon.com

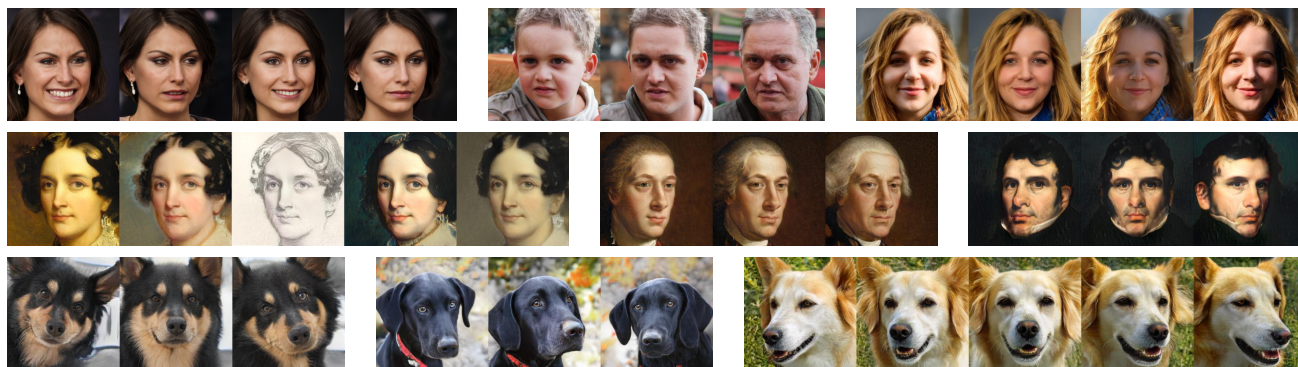Gerard Medioni
Amazon One
medioni@amazon.com

Figure 1: We propose a framework for training GANs in a disentangled manner which allows for explicit control over generation attributes. Our method is applicable to diverse controls in various domains. First row (left to right) demonstrates our control over facial expression, age and illumination of human portraits. Second row (left to right) demonstrates our control over artistic style, age and pose of paintings. Third row demonstrates our pose control over faces of dogs.

Abstract

We present a framework for training GANs with explicit control over generated images. We are able to control the generated image by settings exact attributes such as age, pose, expression, etc. Most approaches for editing GAN-generated images achieve partial control by leveraging the latent space disentanglement properties, obtained implicitly after standard GAN training. Such methods are able to change the relative intensity of certain attributes, but not explicitly set their values. Recently proposed methods, designed for explicit control over human faces, harness morphable 3D face models to allow fine-grained control capabilities in GANs. Unlike these methods, our control is not constrained to morphable 3D face model parameters and is extendable beyond the domain of human faces. Using contrastive learning, we obtain GANs with an explicitly disentangled latent space. This disentanglement is utilized to train control-encoders mapping human-interpretable inputs to suitable latent vectors, thus allowing explicit control. In the domain of human faces we demonstrate control over identity, age, pose, expression, hair color and illumination. We also demonstrate control capabilities of our framework in the domains of painted portraits and dog image genera-tion. We demonstrate that our approach achieves state-of-the-art performance both qualitatively and quantitatively.

1. Introduction

Generating controllable photorealistic images has applications spanning a variety of fields such as cinematography, graphic design, video games, medical imaging, virtual communication and ML research. For face images especially, impressive breakthroughs were made. As an example, in movies, computer generated characters are replacing live actor footage. Earlier work on controlled face generation primarily relied on 3D face rig modeling [31, 39], controlled by 3D morphable face model parameters, such as 3DMM [7, 16]. While being easily controllable, such methods tend to suffer from low photorealism. Other methods that rely on 3D face scanning techniques may provide highly photorealistic images, but at a high cost and limited variability. Recent works on generating high resolution images using generative adversarial networks (GANs) [18] have demonstrated the ability to generate photorealistic faces of novel identities, indistinguishable from real human faces [26, 28, 29]. However, these methods alone lack in-

1

terpretability and control over the outcome of the generative process as compared to the 3D graphic alternatives.

These results have inspired the community to explore ways to benefit from both worlds – generating highly photorealistic faces using GANs while controlling their fine-grained attributes, such as pose, illumination and expression with 3DMM-like parameters. Deng *et al*. [13], Kowalski *et al*. [30] and Tewari *et al*. [44] introduce explicit control over GAN-generated faces, relying on guidance from 3D face generation pipelines. Along with the clear benefits, such as the precise control and perfect ground truth, reliance on such 3D face models introduce new challenges. For example, the need to overcome the synthetic-to-real domain gap [30, 13]. Finally, all these methods' expressive power is bounded by the capabilities of the model they rely on. In particular, it is not possible to control human age if the 3D modeling framework does not support it. It is also impossible to apply the same framework to different but similar domains, such as paintings or animal faces, if these assets are not supported by the modeling framework. All of these stand in the way of creating a simple, generic and extendable solution for explicitly controllable GANs.

In this work we present a unified approach for training a GAN to generate high-quality, controllable images. Specifically, we demonstrate our approach in the domains of facial portrait photos, painted portraits and dogs (see Fig. 1). We depart from the common use of the highly detailed 3D face models in favor of supervision signals provided by a set of pre-trained models, each controlling a different feature. We show that our approach significantly simplifies the generation framework, does not compromise image quality or control accuracy, and allows us to control additional aspects of facial appearances, which can't be modeled by graphical pipelines. We achieve this by applying contrastive loss terms [19] for the controllable attributes of the generated image pairs. That is, we constructs the GAN's latent space as a composition of sub-spaces, each corresponding to a specific property. During training, we enforce that images generated by identical latent sub-vectors have similar properties, as predicted by some off-the-shelf model. Conversely, images generated by different latent sub-vectors should have different predicted properties. To allow for human-interpretable control, for each attribute we train an encoder converting values from its feasible range to the latent space. Finally, we present a novel image projection approach suitable for disentangled latent spaces. Our approach takes advantage of this disentanglement to find a latent vector that both reconstructs the image accurately and remains in the semantically meaningful manifold. This allows us to edit properties of real images using our GAN's controls.

We summarize our contributions as following:

1. We present a novel state-of-the art approach for train-

ing explicitly controllable, high-resolution GANs.

2. Our approach is extendable to attributes beyond those supported by 3D modeling and rendering frameworks, making it applicable to additional domains.

3. We present a disentangled projection method that enables real image editing.

2. Related work

Generative adversarial networks [18] introduced new possibilities to the field of image generation and synthesis. Currently, state-of-the-art GANs [29, 28, 26, 8] can produce high-resolution synthetic images that are indistinguishable from real images. GANs are also employed in supervised and unsupervised image-to-image translation [24, 45, 35, 49, 9, 34, 23, 10] allowing to transform or edit a given image in various imaginative ways.

Our work focuses on controllable *de novo* image generation, but also allows editing real images via projection to latent space.

Implicit control over image generation   A widely studied approach for controlling the generated images of GANs is by exploiting the inherent disentanglement properties of the GAN's latent space [25, 46, 20, 40, 6]. Härkönen *et al*. [20] identify latent directions based on principal component analysis (PCA) in latent space that correspond to image attributes. Control can be obtained by traversing the latent space along these directions. Shen *et al*. [40] use off-the-shelf binary classifiers to find separation boundaries in the latent space where each side of the boundary corresponds to an opposite semantic attribute (*e.g*. young vs. old). Pushing a latent vector towards or away from a boundary translates to increasing or decreasing the corresponding image attribute. While simple, these methods may exhibit entanglement, *i.e*., changing one attribute affects others. In [15, 41] the above is mitigated by explicitly disentangling the GAN's latent space during training. All of the above methods, while providing solutions to edit generated images by some guidance signal (*e.g*., turn the face older or rotate the face towards the left, *etc*.), do not provide explicit control (*e.g*., generate a 40 years old face, rotated 30° to the left, *etc*.).

Explicit control over image generation   Recently, three novel methods were proposed to allow explicit control over *de novo* face image generation: StyleRig [44], DiscoFaceGAN [13] (DFG), and CONFIG [30]. These methods propose solutions for translating controls of 3D face rendering models to GAN-generating processes. Both StyleRig and
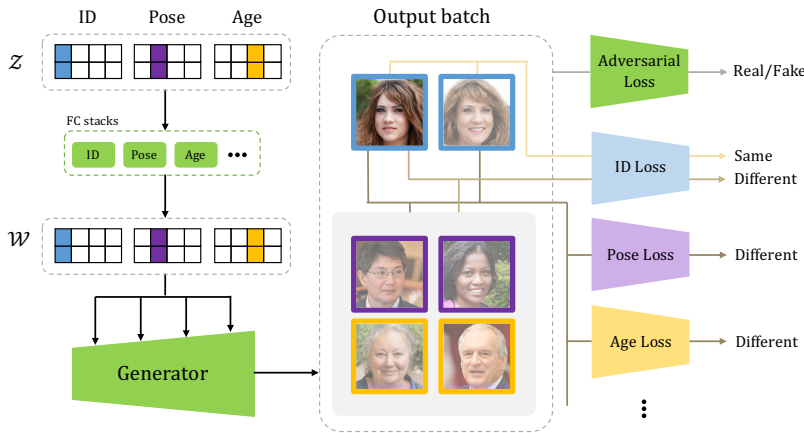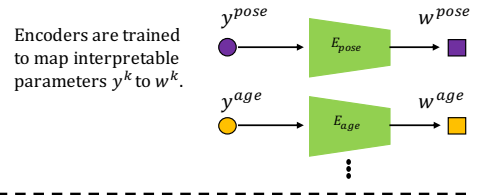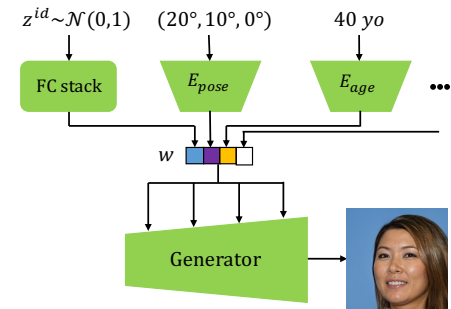
Figure 2: **Explicitly controllable GAN**: In Phase 1, we construct every batch so that for each attribute, there is a pair of latent vectors sharing a corresponding sub-vector, $\mathbf{z}^k$. In addition to the adversarial loss, each image in the batch is compared in a contrastive manner, attribute-by-attribute, to all others, taking into account if it has the same or a different sub-vector. In Phase 2, encoders are trained to map interpretable parameters to suitable latent vectors. Inference: An explicit control over the attribute k is achieved by setting the E_k's input to a required value.

DFG utilize 3DMM [7] parameters as controls in the generation framework. This restricts both approaches to provide controls only over the expression, pose and illumination, while preserving identity (ID). CONFIG uses a custom 3D image rendering pipeline to generate an annotated synthetic dataset. This dataset is later used to acquire controls matching the synthetic ground truth, allowing CONFIG to add controls such as hair style and gaze. Producing such datasets is hard and requires professional handcrafted 3D assets. We emphasize that these methods are only applicable in the domain of human faces, and only to the controls parametrized by 3D face models. In contrast to the above methods, our approach does not rely on 3D face rendering frameworks. Rather, it relies on our ability to estimate such properties. In the age of open-source deep learning research, many models predicting such properties are readily available.

3. Proposed approach

In this section we present our framework for training explicitly controllable GANs. Our approach is simple yet effective and is comprised of two phases (see Fig. 2):

- **Disentanglement by contrastive learning:** training a GAN with explicitly disentangled properties. As a result, the latent space is divided into sub-spaces, each encoding a different image property.

- **Interpretable explicit control:** for each property, an MLP encoder is trained to map control parameter values to a corresponding latent sub-space. This enables explicit control over each one of the properties.

3.1. Disentanglement by contrastive learning

The approach builds on the StyleGAN2 [29] architecture. Initially, we divide both latent spaces, $\mathcal{Z}$ and $\mathcal{W}$ to $N+1$ separate sub-spaces, $\{\mathcal{Z}^k\}_{k=1}^{N+1}$, and $\{\mathcal{W}^k\}_{k=1}^{N+1}$, where N is the number of control properties. Each sub-space is associated with an attribute (*e.g.*, ID, age etc.) except for the last one. Similarly to Deng *et al.* [13] the last sub-space encodes the rest of the image properties that are not controllable. We modify the StyleGAN2 architecture so that each control has its own 8-layered MLP. We denote $\mathbf{z} = (\mathbf{z}^1\mathbf{z}^2 \ldots \mathbf{z}^{N+1})$ and $\mathbf{w} = (\mathbf{w}^1\mathbf{w}^2 \ldots \mathbf{w}^{N+1})$ the concatenation of the sub-vectors in both latent spaces. The combined latent vector, $\mathbf{w}$, is then fed into the generator of StyleGAN2.

Next, we describe how we enforce disentanglement during training. Let $\mathcal{I}_i = G(\mathbf{z}_i)$ denote an image generated from a latent vector $\mathbf{z}_i$ and let $B = \{\mathbf{z}_i\}_{i=1}^{N_B}$ denote a latent vector batch of size N_B. We define our factorized-contrastive loss as:

$$L_c = \sum_{\substack{\mathbf{z}_i, \mathbf{z}_j \in B \\ i \neq j}} \sum_{k=1}^{N} l_k(\mathbf{z}_i, \mathbf{z}_j), \tag{1}$$

3

where l_k is a contrastive loss component for attribute k. We define the per-attribute contrastive loss as,

$$l_k(\mathbf{z}_i, \mathbf{z}_j) = \begin{cases} \frac{1}{C_k^+} \max\left(d_k(\mathcal{I}_i, \mathcal{I}_j) - \tau_k^+, 0\right), & \mathbf{z}_i^k = \mathbf{z}_j^k \\ \frac{1}{C_k^-} \max\left(\tau_k^- - d_k(\mathcal{I}_i, \mathcal{I}_j), 0\right), & \text{otherwise} \end{cases} \quad (2)$$

where $\mathbf{z}_i^k$ denotes the k-th sub-vector of $\mathbf{z}_i$, d_k is the distance function for attribute k, $\tau_k^\pm$ are the per-attribute thresholds associated with same and different sub-vectors and $C_k^\pm$ are constants that normalize the loss according to the number of same and different loss components, *i.e.* $C_k^+ = \sum_{i,j} \mathbb{1}\{\mathbf{z}_i^k = \mathbf{z}_j^k\}$ and $C_k^- = \sum_{i,j} \mathbb{1}\{\mathbf{z}_i^k \neq \mathbf{z}_j^k\}$.

We construct each training batch to contain pairs of latent vectors that share one sub-vector, *i.e.*, for each attribute, $k \in \{1, \dots, N\}$, we create a pair of latent vectors, $\mathbf{z}_i$ and $\mathbf{z}_j$, where $\mathbf{z}_i^k = \mathbf{z}_j^k$ and $\mathbf{z}_i^r \neq \mathbf{z}_j^r$ for $r \in \{1, \dots, N{+}1\}, r \neq k$. For example, let us assume that the generator has produced a batch of size $N_b > 2$, where images $\mathcal{I}_0$ and $\mathcal{I}_1$ share the same $\mathbf{z}^{ID}$ (see the pair of images with the blue frame in Fig. 2). The ID component of the contrastive loss, l_{ID}, will penalizes the dissimilarities between the $\mathcal{I}_0$'s and $\mathcal{I}_1$'s IDs and the similarities between $\mathcal{I}_0$'s or $\mathcal{I}_1$'s ID to the IDs of all other images in the batch. The other loss components (age, pose, *etc.*) will penalize for similarity between $\mathcal{I}_0$ and any other image in the batch. The losses for all other images in the batch are constructed in the same manner.

To be able to control a specific attribute of the generated image, we assume that we are given access to a differentiable function $M_k : \mathcal{I} \to \mathbb{R}^{D_k}$, mapping an image to a D_k-dimensional space. We assume that the projected images with similar attribute values fall close to each other, and images with different attribute values fall far from one another. Such requirements are met by most neural networks trained with either a classification or a regression loss – for example, a model estimating the head pose or the person's age. We define the k's attribute distance between two images $\mathcal{I}_i$ and $\mathcal{I}_j$ as their distance in the corresponding embedding space:

$$d_k(\mathcal{I}_i, \mathcal{I}_j) = dist(M_k(\mathcal{I}_i), M_k(\mathcal{I}_j)), \quad (3)$$

where $dist(\cdot, \cdot)$ is a distance metric, *e.g.*, L_1, L_2, cosine-distance, *etc*. For example, to capture the ID property, a face recognition model, M_{ID}, is used to extract embedding vectors from the generated images. Then, the distances between the embedding vectors are computed using the cosine-distance.

In Section 4 we demonstrate that as the result of training with this architecture and batch sampling protocol, we achieve disentanglement in the GAN's latent space. While such disentanglement allows to assign a randomly sampled value to each individual attribute, independently of the others, additional work is required for turning such control explicit and human-interpretable, *e.g.*, generate a human face image with a specific user-defined age.

3.2. Interpretable explicit control

We propose a simple procedure to allow explicit control of specific attributes. We train a mapping $E_k : y^k \to \mathbf{w}^k$, where y^k is a human-interpretable representation of the attribute (*e.g.*, age = 20yo, pose = $(20°, 5°, 2°)$, *etc.*). Given a trained disentangled GAN, we train N encoders $\{E_k\}_{k=1}^N$, one for each attribute (see Training-Phase 2 in Fig. 2). Then, at inference time we can synthesize images using any combination of sub-vectors $\{\mathbf{w}^k\}_{k=1}^{N+1}$, where $\mathbf{w}^k$ is either controlled explicitly using E_k or sampled from $\mathbf{z}^k$ and consequently mapped to $\mathbf{w}^k$ (see Inference in Fig. 2).

To train the control encoders, we randomly sample N_s latent vectors $\{\mathbf{z}_i\}_{i=1}^{N_s}$ and map them to the intermediate latent vectors, $\{\mathbf{w}_i\}_{i=1}^{N_s}$. Then, for each attribute, k, we map $\mathbf{z}_i$, to a predicted attribute value, $y_i^k = M_k(G(\mathbf{z}_i))$. Thus we obtain N distinct datasets $\{\{\mathbf{w}_i^k, y_i^k\}_{i=1}^{N_s}\}_{k=1}^N$, where for each intermediate sub-vector $\mathbf{w}^k$ there is a corresponding attribute predicted from the image it produced. We then train N encoders, each on its corresponding dataset. In our experiments we show that despite its simplicity, our encoding scheme does not compromise control accuracy compared to other methods.

4. Experiments

In this section we present experiments on several domains that demonstrate the flexibility of the proposed approach. We quantitatively compare our approach to recent published approaches.

4.1. Face generation

Implementation details: We use the FFHQ dataset [28] downsampled to 512x512 resolution. The latent spaces $\mathcal{Z}$ and $\mathcal{W}$ are divided into the following sub-spaces: ID, pose, expression, age, illumination, hair color and an additional "other" sub-space. Next, we list the models, M_k, that were used to compute the distance measures, d_k, for each one of the attributes. For the ID, head-pose, expression, illumination, age and hair color we used Arc-Face [12], Ruiz *et al.* [38], ESR [43], the γ output of R-Net [14], Dex [37], average color of hair segmented by PSPNet [47], respectively (additional details in supplementary material). In the second phase (Section 3.2), we train five encoders ($E_{pose}, E_{exp}, E_{age}, E_{illum}, E_{hair}$), each composed of a 4-layered MLP. The input to our control encoder is defined as follows – $y^{age} \in [15, 75]$ years-old (yo), $y^{pose} \in [-90°, 90°]^3$ is represented by the Euler angles $\theta = \{\text{Pitch}, \text{Yaw}, \text{Roll}\}$, $y^{illum} \in \mathbb{R}^{27}$ is represented by the γ Spherical Harmonics (SH) coefficients approximating scene illumination [36], $y^{exp} \in \mathbb{R}^{64}$ is represented by the β expression coefficients of the 3DMM [7] model, $y^{hair} \in [0, 255]^3$ is represented by the mean-color RGB values.
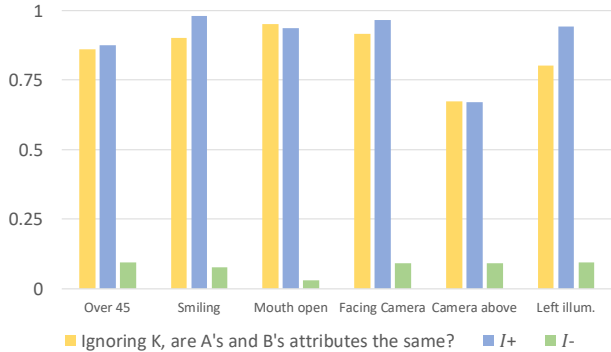
4

Figure 3: **Disentanglement user study:** Blue and green bars show whether users agree that a given attribute is present or lacking in images ($\mathcal{I}_+$, $\uparrow$), ($\mathcal{I}_-$, $\downarrow$) respectively. The yellow bars measure whether the users agree that the other attributes are maintained.

GAN	Ours	DFG [13]	CONFIG [30]
Version	512x512	256x256	256x256
Vanilla	3.32	5.49	33.41
Controlled	5.72	12.9	39.76

Table 1: **FID↓ score for different methods on FFHQ:** second row shows the dataset resolution. Note that the FID scores cannot be compared between columns since every method uses different pre-processing for the FFHQ dataset (*e.g.*, image size, alignment, cropping).

	Ours	DFG	CONFIG
Synthetic comparison	**67%**	22%	11%
Synthetic vs. real	**47%**	27%	16%

Table 2: **Photorealism user studies↑:** (First row) users were asked to vote for the most realistic image from triplets of synthetic images (Ours, DFG, CONFIG). (Second row) users were shown pairs of images – one synthetic and one from the FFHQ dataset – and were asked to choose the real one from the two.

Photorealism: Table 1 shows FID [22] scores of Disco-FaceGAN [13], CONFIG [30] (image resolution 256x256) and our approach (image resolution 512x512). The table also shows the FID of the corresponding baseline GANs: StyleGAN [28], HoloGAN [33] and StyleGAN2 [29]. Our FID score is calculated without the use of the truncation trick [8, 28]. For DFG and CONFIG the FID score is taken from the corresponding papers. Similarly to the other works, we observe a deterioration in FID when control is introduced. However, due to the different image resolutions and data pre-processing steps, the numbers are not directly comparable. To make a clear image quality comparison between all three methods, we conducted two photorealism

Control	Ours	DFG	CONFIG	FFHQ
Pose [°]	$2.29_{\pm 1.31}$	$3.92_{\pm 2.1}$	$6.9_{\pm 4.7}$	$23.8_{\pm 14.6}$
Age [yo]	$2.02_{\pm 1.38}$	N/A	N/A	$16.95_{\pm 12.9}$
Exp.	$3.68_{\pm 0.7}$	$4.07_{\pm 0.7}$	N/A[a]	$4.45_{\pm 0.9}$
Illum.	$0.32_{\pm 0.13}$	$0.29_{\pm 0.1}$	N/A[a]	$0.62_{\pm 0.2}$
Hair color	$0.13_{\pm 0.18}$	N/A	N/A[a]	$0.34_{\pm 0.25}$

Table 3: **Control precision↓:** Comparison of average distance between input controls to resulted image attribute. Last column shows the average distance between random samples in the FFHQ dataset.

---

[a]CONFIG uses different controls for expression, illumination and hair color.

ID	Ours	Ours$_{+age}$	DFG	CONFIG
Same↓	$\mathbf{0.68_{\pm 0.19}}$	$0.75_{\pm 0.2}$	$0.83_{\pm 0.3}$	$1.07_{\pm 0.29}$
Not same↑	$\mathbf{1.9_{\pm 0.24}}$	$\mathbf{1.9_{\pm 0.24}}$	$1.73_{\pm 0.24}$	$1.63_{\pm 0.25}$

Table 4: **Identity preservation:** First row shows the mean embedding distance between generated images with the same $\mathbf{z}^{ID}$ (in Ours$_{+age}$, $\mathbf{z}^{age}$ is also changed). Second row shows the mean embedding distance between randomly generated images. For comparison, the mean embedding distance between 10K FFHQ images is 1.89 ± 0.21.

user studies, using Amazon Mechanical Turk. In the first, users were shown 1K triplets of synthetic images, one from each method in a random order. Users were asked to vote for the most realistic image of the three. Each triplet was evaluated by three participants. In the second study, users were shown 999 pairs of images. Each pair contains one real image from the FFHQ dataset and an image generated by one of the three methods. For each method, 333 image pairs were evaluated by three different users. All the synthetic images in this experiment were generated using the truncation trick with $\Psi = 0.7$ (our and DFG use the attribute-preserving truncation trick [13]) and all images were resized to 256x256 resolution. From Table 2 it is evident that our method achieves the highest photorealism. Surprisingly, our method reaches a near perfect result of 47% when compared to FFHQ, *i.e.*, users were barely able to distinguish between our images and the ones from FFHQ in terms of photorealism. We note that differences in image quality may depend on the base model that was used (HoloGAN, StyleGAN, StyleGAN2).

Explicit control analysis: To validate that we indeed have an explicit control over the output of our model, we perform a control precision comparison. 10K images are randomly chosen from FFHQ and their attributes are predicted to produce a pool of feasible attributes that appear in real images. For each attribute in the pool, y_i^k, we generate a corresponding image. Then, we predict the attribute value
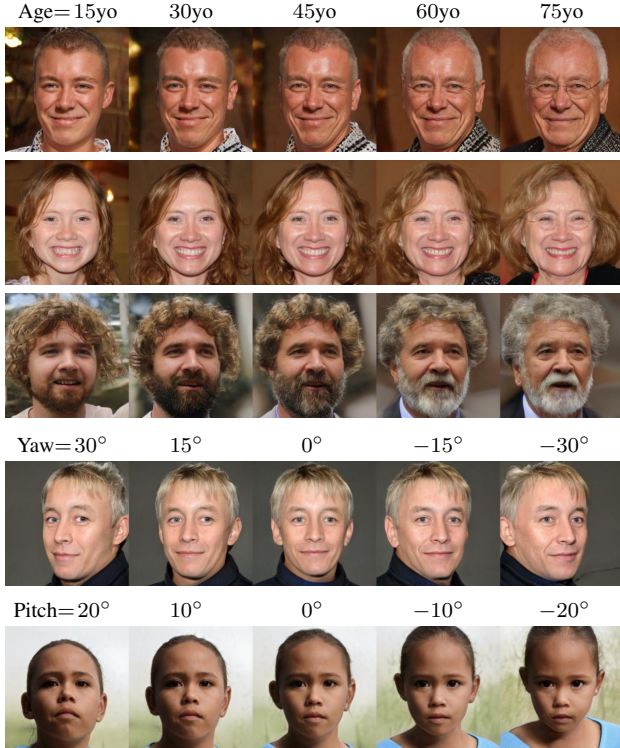
Age= 15yo | 30yo | 45yo | 60yo | 75yo

Yaw= 30° | 15° | 0° | −15° | −30°

Pitch= 20° | 10° | 0° | −10° | −20°

Figure 4: **Controlling age and pose:** Rows 1-3 show generation results using E_{age}. Rows 4-5 show generation results using E_{pose}.

Illum. 1 | Illum. 2 | Illum. 3 | Illum. 4 | Illum. 5

Exp. 1 | Exp. 2 | Exp. 3 | Exp. 4 | Exp. 5
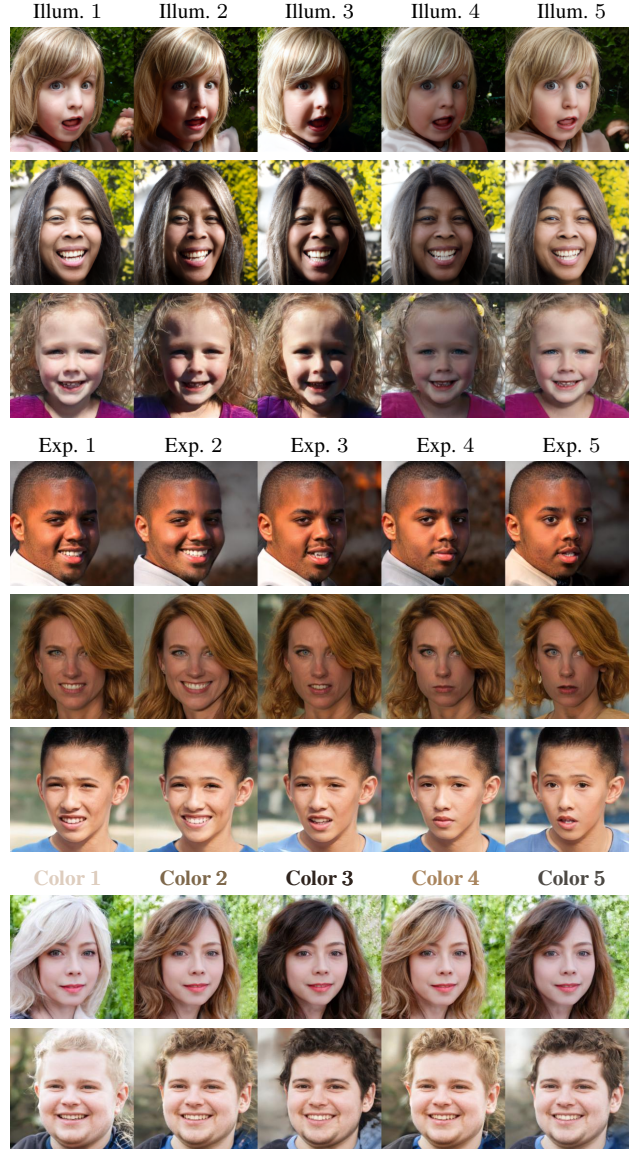
Color 1 | Color 2 | Color 3 | Color 4 | Color 5

Figure 5: **Controlling illumination, expression and hair color:** Rows 1-3 show generation results using E_{illum}. Rows 4-6 show generation results using E_{exp}. Rows 7-8 show generation results using E_{hair}. Each column has the same attribute matching the control input.

from the generated image, $\hat{y}_i^k$, and measure the Euclidean distance between the two. More details are provided in the supplementary material. Table 3 shows the comparison of the control precision between the methods. The results demonstrate that we can achieve an explicit control of the attributes that is comparable or better than other methods.

ID preservation analysis: We use ArcFace [12] to extract embedding vectors of generated images to compare identity preservation to other methods. This is done by generating 10K image pairs that share the ID attribute and have different pose, illumination and expression attributes. We choose to modify these as they are common to all three methods. To demonstrate the ability of our method to preserve the ID even at different ages, we report results for Ours$_{+age}$ where each image in a pair is generated using different a $\mathbf{z}^{age}$ vector. The results presented in Table 4 demonstrate that our method achieves the highest identity preservation.

Disentanglement user study: We conducted a user study similar to the one reported in CONFIG [30]. For each attribute, k, we generate a pair of images, $\mathcal{I}_+, \mathcal{I}_-$. The attribute for $\mathcal{I}_+$ is set to y_+^k (*e.g.*, smiling face) and the attribute for $\mathcal{I}_-$ is set to a semantically opposite value y_-^k (*e.g.*, sad face). Users are then asked to evaluate the presence of

y_+^k in $\mathcal{I}_+$ and $\mathcal{I}_-$ on a 5-level scale. In addition, for every pair of images the users are asked to evaluate to what extent all other attributes, apart from k, are preserved. In total, 50 users have evaluated 1300 pairs of images. Fig. 3 clearly shows that the attributes of the generated images are perceived as disentangled.

Qualitative evaluation: Next we show editing results of generated images via the control encoders E_k. Fig. 4 shows explicit control over age and pose of faces using E_{age}

Figure 6: **Control of paintings:** Generation results using E_{age}, E_{pose} and E_{exp}.

and E_{pose}. Interestingly, as the age is increased the model tends to generate glasses as well as more formal clothing. Two other prominent features are graying of the hair and the addition of wrinkles. Fig. 5 shows control over illumination and expression using E_{illum} and E_{exp}.

4.2. Painting generation

Implementation details: We use MetFaces [27], 1,336 images downsampled to 512x512 resolution. In addition to the traditional StyleGAN2 and our explicit disentanglement training schemes, we use the method of non-leaking augmentation by Karras *et al.* [27] for training GANs with limited data. We use the same M_k models as in our face generation scheme with the following modifications: (1) the illumination and hair color controls are removed, (2) a control for image style is added. The style similarity distance d_{style} is computed similarly to the style loss introduced for style transfer by Gatys *et al.* [17] where M_{style} is a VGG16 [42] network pre-trained on ImageNet [11].

Photorealism: The FID scores are 28.58 and 26.6 for our controlled and for the baseline models, respectively.

Figure 7: **Artistic style for paintings:** We can change the $\mathbf{z}^{style}$ latent to produce same portraits with different style.

Qualitative evaluation: Fig. 6 shows our control over age, pose and expression using E_{age}, E_{pose} and E_{exp}. Note that the expression control for this task is rather limited. We suspect this is due to the low variety of expressions in the dataset. The control over these attributes demonstrates that the control networks do not necessarily need to be trained on the same domain on which the GAN is being trained, and that some domain gap is tolerable. Fig. 7 shows that our method can also disentangle artistic style allowing to change the style without affecting the rest of the attributes.

4.3. Dog generation

In this experiment we aim to control the identity and pose of dogs, to demonstrate our capability to generalize to additional domains other than human faces.

Implementation details: We use AFHQ [10], 5,239 dog face images downsampled to 512x512 resolution. We use StyleGAN2 with non-leaking augmentation [27] as before, for paintings. For preserving dog IDs we use two different models (M_{ID}^0, M_{ID}^1). M_{ID}^0 is a dog-face recognition model DogFaceNet [32]. We noticed that DogFaceNet often recognizes two dogs to be the same if a similar pattern is present on their heads, even if they are of different breeds. To overcome this issue, we use ResNet18 [21] trained on ImageNet [11] as M_{ID}^1 (the penultimate layer is used for the distance comparison). We use this model since of the 1K classes in the ImageNet challenge, 90 are dog-breeds. For M_{pose} we use the same pose detection network as for human faces and paintings [38].

Photorealism: The FID scores are 8.74 and 8.22 for our controlled and for the baseline models, respectively.

Qualitative evaluation: Fig. 8 shows precise control over dog pose using E_{pose}. We show that the pose estimation network was able to provide enough guidance to the GAN even though the domain gap between dog and human faces is quite large. Since dogs are rarely photographed from below, our model was not able to generate images of dogs with a positive pitch. Unlike humans, dogs exhibit a large variability in head-roll, therefore the model was able to capture this aspect well.
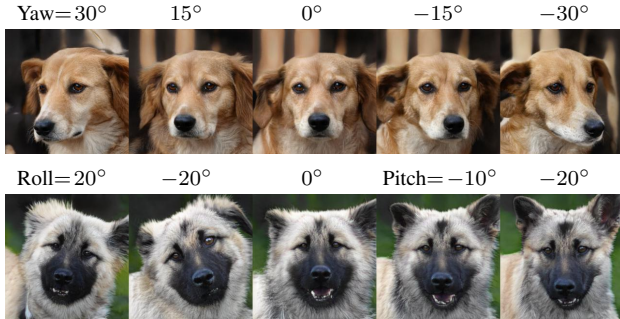
Figure 8: **Controlling head pose in dog images:** Generation results using E_{pose}.

4.4. Disentangled projection of real images

We leverage the explicit control of our model for real image editing. To this end, we use latent space optimization to find a latent vector that corresponds to an input image. By naïvely following the projection method described in StyleGAN2 (Appendix D), the reconstructed image visually looks different from the input image. A remedy to this phenomenon proposed in [5] is to project the image to an extended latent space, w^+, such that each resolution level has its own latent vector. We find this approach is indeed useful for accurate reconstruction. However, when we modified the different sub-vectors, we observed a strong deterioration in the image quality and a change in other unmodified attributes. In absence of explicit constraints on the feasible solutions' space, two different issues arise: (1) part of the sub-vectors end-up encoding a semantically different information from the one they were intended for, *e.g.*, the pose latent vector may encode some information of the ID or the expression, and (2) the reconstructed latent vector may not lie in the semantically meaningful manifold. A similar phenomenon was reported in Zhu *et al.* [48]. As a mitigation to the above, we introduce two changes. First, rather than extending the entire $\mathcal{W}$ space, we only extend the $\mathcal{W}^{ID}$ and $\mathcal{W}^{other}$ sub-spaces. Second, we constrain the remaining sub-vectors to reside on approximated linear subspaces of their corresponding manifolds. We achieve this using the following approach: we perform PCA for each latent subspace of 10K randomly sampled sub-vectors $\mathbf{w}$, where the number of components are selected so as to preserve 50% of the variance. During the optimization process, we project the latent sub-vectors to the truncated PCA spaces and re-project them back to the corresponding spaces. Once we find the corresponding latent vector, we can edit the image by modifying attribute k latent sub-vector, using E_k. We provide an ablation study of the proposed changes in the supplementary material.

In Fig. 9 we show real images, their projections and the result of editing of their attributes. While the projected im-
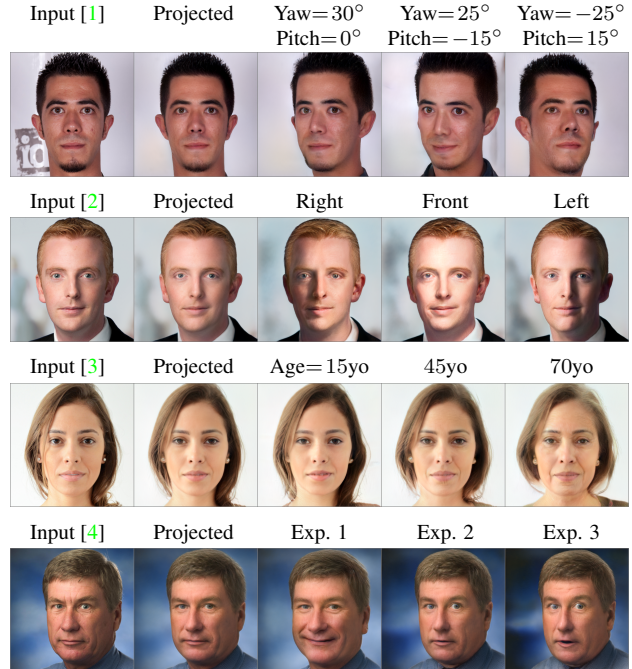

Figure 9: **Disentangled Projection:** The two leftmost columns refer to the input and projected images, respectively. The remaining columns demonstrate editing results of pose, illumination, age and expression.

age does not achieve a perfect reconstruction, the disentanglment of the latent space is preserved, allowing for an explicit control of the desired attributes without affecting others. In the second row of Fig. 9 we can see that the GAN can accurately model the shadows on the face's curvature and skin folds as well as model the reflection of the light source in the person's eyes. This implies the GAN learns a latent 3D representation of the faces.

In the supplementary we present method analyses, additional resulted, method limitations and provide implementation details.

5. Conclusions

We proposed a novel framework for training GANs in a disentangled manner, that allows explicit control over generation attributes. For a variety of attributes, a predictor of that attribute is enough to achieve explicit control over it. Our method extends the applicability of explicitly controllable GANs to additional domains other than human faces. The GAN is complemented by a real image projection method that projects images to a disentangled latent space, maintaining explicit control. We believe this work opens up a path for improving the ability to control general-purpose GAN generation. More details can be found on our project page.

References

[1] The original image is at http://www.flickr.com/photos/quakecon/3923570806 and is licensed under: http://www.creativecommons.org/licenses/by/2.0. 8

[2] The original image is at http://www.flickr.com/photos/dereknolan/5309847731 and is licensed under: http://www.creativecommons.org/licenses/by/2.0. 8

[3] The original image is at http://www.flickr.com/photos/67548743@N02/6854926480 and is licensed under: http://www.creativecommons.org/licenses/by/2.0. 8

[4] The original image is at http://www.flickr.com/photos/ugacommunications/6005899336 and is licensed under: http://www.creativecommons.org/licenses/by-nc/2.0. 8

[5] Rameen Abdal, Yipeng Qin, and Peter Wonka. Image2stylegan: How to Embed Images Into the StyleGAN Latent Space? In *Proceedings of the IEEE/CVF International Conference on Computer Vision (ICCV)*, October 2019. 8

[6] Guha Balakrishnan, Yuanjun Xiong, Wei Xia, and Pietro Perona. Towards Causal Benchmarking of Bias in Face Analysis Algorithms. 2020. 2

[7] Volker Blanz and Thomas Vetter. A Morphable Model for the Synthesis of 3D Faces. In *Proceedings of the 26th Annual Conference on Computer Graphics and Interactive Techniques*, pages 187–194, 1999. 1, 3, 4

[8] Andrew Brock, Jeff Donahue, and Karen Simonyan. Large Scale GAN Training for High Fidelity Natural Image Synthesis. In *International Conference on Learning Representations*, 2019. 2, 5

[9] Yunjey Choi, Minje Choi, Munyoung Kim, Jung-Woo Ha, Sunghun Kim, and Jaegul Choo. StarGAN: Unified Generative Adversarial Networks for Multi-Domain Image-to-Image Translation. In *Proceedings of the IEEE Conference on Computer Vision and Pattern Recognition CVPR*, 2018. 2

[10] Yunjey Choi, Youngjung Uh, Jaejun Yoo, and Jung-Woo Ha. StarGAN v2: Diverse Image Synthesis for Multiple Domains. In *Proceedings of the IEEE Conference on Computer Vision and Pattern Recognition CVPR*, 2020. 2, 7

[11] J. Deng, W. Dong, R. Socher, L.-J. Li, K. Li, and L. Fei-Fei. ImageNet: A Large-Scale Hierarchical Image Database. In *IEEE/CVF Conference on Computer Vision and Pattern Recognition (CVPR)*, 2009. 7

[12] Jiankang Deng, Jia Guo, Niannan Xue, and Stefanos Zafeiriou. ArcFace: Additive Angular Margin Loss for Deep Face Recognition. In *Proceedings of the IEEE Conference on Computer Vision and Pattern Recognition*, pages 4690–4699, 2019. 4, 6

[13] Yu Deng, Jiaolong Yang, Dong Chen, Fang Wen, and Xin Tong. Disentangled and Controllable Face Image Generation via 3D Imitative-Contrastive Learning. In *IEEE Computer Vision and Pattern Recognition*, 2020. 2, 3, 5

[14] Yu Deng, Jiaolong Yang, Sicheng Xu, Dong Chen, Yunde Jia, and Xin Tong. Accurate 3D Face Reconstruction with Weakly-Supervised Learning: from Single Image to Image Set. In *IEEE Computer Vision and Pattern Recognition Workshops*, 2019. 4

[15] Chris Donahue, Zachary C Lipton, Akshay Balsubramani, and Julian McAuley. Semantically Decomposing the Latent Spaces of Generative Adversarial Networks. In *ICLR*, 2018. 2

[16] Bernhard Egger, William AP Smith, Ayush Tewari, Stefanie Wuhrer, Michael Zollhoefer, Thabo Beeler, Florian Bernard, Timo Bolkart, Adam Kortylewski, Sami Romdhani, et al. 3D Morphable Face Models—Past, Present, and Future. *ACM Transactions on Graphics (TOG)*, 39(5):1–38, 2020. 1

[17] Leon A Gatys, Alexander S Ecker, and Matthias Bethge. Image Style Transfer Using Convolutional Neural Networks. In *CVPR*, 2016. 7

[18] Ian Goodfellow, Jean Pouget-Abadie, Mehdi Mirza, Bing Xu, David Warde-Farley, Sherjil Ozair, Aaron Courville, and Yoshua Bengio. Generative Adversarial Nets. In *Advances in Neural Information Processing Systems*, pages 2672–2680, 2014. 1, 2

[19] Raia Hadsell, Sumit Chopra, and Yann LeCun. Dimensionality Reduction by Learning an Invariant Mapping. In *2006 IEEE Computer Society Conference on Computer Vision and Pattern Recognition (CVPR'06)*, volume 2, pages 1735–1742. IEEE, 2006. 2

[20] Erik Härkönen, Aaron Hertzmann, Jaakko Lehtinen, and Sylvain Paris. Ganspace: Discovering Interpretable GAN Controls. *arXiv preprint arXiv:2004.02546*, 2020. 2

[21] Kaiming He, X. Zhang, Shaoqing Ren, and Jian Sun. Deep Residual Learning for Image Recognition. *2016 IEEE Conference on Computer Vision and Pattern Recognition (CVPR)*, pages 770–778, 2016. 7

[22] Martin Heusel, Hubert Ramsauer, Thomas Unterthiner, Bernhard Nessler, and Sepp Hochreiter. Gans Trained by a Two Time-Scale Update Rule Converge to a Local Nash Equilibrium. In *NIPS*, 2017. 5

[23] Xun Huang, Ming-Yu Liu, Serge Belongie, and Jan Kautz. Multimodal Unsupervised Image-to-Image Translation. In *ECCV*, 2018. 2

[24] Phillip Isola, Jun-Yan Zhu, Tinghui Zhou, and Alexei A Efros. Image-to-Image Translation with Conditional Adversarial Networks. *CVPR*, 2017. 2

[25] Ali Jahanian, Lucy Chai, and Phillip Isola. On the "Steerability" of Generative Adversarial Networks. In *International Conference on Learning Representations*, 2020. 2

[26] Tero Karras, Timo Aila, Samuli Laine, and Jaakko Lehtinen. Progressive Growing of GANs for Iimproved Quality, Stability, and Variation. *arXiv preprint arXiv:1710.10196*, 2017. 1, 2

[27] Tero Karras, Miika Aittala, Janne Hellsten, Samuli Laine, Jaakko Lehtinen, and Timo Aila. Training generative adversarial networks with limited data. *arXiv preprint arXiv:2006.06676*, 2020. 7

[28] Tero Karras, Samuli Laine, and Timo Aila. A Style-Based Generator Architecture for Generative Adversarial Networks. In *Proceedings of the IEEE Conference on Computer Vision and Pattern Recognition CVPR*, pages 4401–4410, 2019. 1, 2, 4, 5

[29] Tero Karras, Samuli Laine, Miika Aittala, Janne Hellsten, Jaakko Lehtinen, and Timo Aila. Analyzing and Improving the Image Quality of StyleGAN. *CoRR*, abs/1912.04958, 2019. 1, 2, 3, 5

[30] Marek Kowalski, Stephan J. Garbin, Virginia Estellers, Tadas Baltrušaitis, Matthew Johnson, and Jamie Shotton. CONFIG: Controllable Neural Face Image Generation. In *European Conference on Computer Vision (ECCV)*, 2020. 2, 5, 6

[31] Tianye Li, Timo Bolkart, Michael J Black, Hao Li, and Javier Romero. Learning a Model of Facial Shape and Expression from 4D Scans. *ACM Trans. Graph.*, 36(6):194–1, 2017. 1

[32] Guillaume Mougeot, Dewei Li, and Shuai Jia. A Deep Learning Approach for Dog Face Verification and Recognition. In *PRICAI 2019: Trends in Artificial Intelligence*, pages 418–430, Cham, 2019. Springer International Publishing. 7

[33] Thu Nguyen-Phuoc, Chuan Li, Lucas Theis, Christian Richardt, and Yong-Liang Yang. HoloGAN: Unsupervised Learning of 3D Representations From Natural Images. In *The IEEE International Conference on Computer Vision (ICCV)*, Nov 2019. 5

[34] Ayellet Tal Ori Nizan. Breaking the Cycle - Colleagues are All You Need. In *IEEE Conference on Computer Vision and Pattern Recognition CVPR*, 2020. 2

[35] Taesung Park, Ming-Yu Liu, Ting-Chun Wang, and Jun-Yan Zhu. Semantic Image Synthesis with Spatially-Adaptive Normalization. In *Proceedings of the IEEE Conference on Computer Vision and Pattern Recognition CVPR*, 2019. 2

[36] R. Ramamoorthi and P. Hanrahan. An Efficient Representation for Irradiance Environment Maps. In *SIGGRAPH '01*, 2001. 4

[37] Rasmus Rothe, Radu Timofte, and Luc Van Gool. Dex: Deep Expectation of Apparent Age from a Single Image. In *IEEE International Conference on Computer Vision Workshops (ICCVW)*, December 2015. 4

[38] Nataniel Ruiz, Eunji Chong, and James M. Rehg. Fine-Grained Head Pose Estimation Without Keypoints. In *The IEEE Conference on Computer Vision and Pattern Recognition (CVPR) Workshops*, June 2018. 4, 7

[39] Soubhik Sanyal, Timo Bolkart, Haiwen Feng, and Michael J Black. Learning to Regress 3D Face Shape and Expression from an Image without 3D Supervision. In *Proceedings of the IEEE Conference on Computer Vision and Pattern Recognition*, pages 7763–7772, 2019. 1

[40] Yujun Shen, Jinjin Gu, Xiaoou Tang, and Bolei Zhou. Interpreting the Latent Space of GANs for Semantic Face Editing. In *IEEE/CVF Conference on Computer Vision and Pattern Recognition (CVPR)*, June 2020. 2

[41] Yujun Shen, Ping Luo, Junjie Yan, Xiaogang Wang, and Xiaoou Tang. FaceID-GAN: Learning a Symmetry Three-Player GAN for Identity-Preserving Face Synthesis. In *IEEE Conference on Computer Vision and Pattern Recognition, CVPR 2018*, 2018. 2

[42] Karen Simonyan and Andrew Zisserman. Very Deep Convolutional Networks for Large-Scale Image Recognition. In *3rd International Conference on Learning Representations, ICLR, year = 2015*. 7

[43] Henrique Siqueira, Sven Magg, and Stefan Wermter. Efficient Facial Feature Learning with Wide Ensemble-based Convolutional Neural Networks, Feb 2020. 4

[44] Ayush Tewari, Mohamed Elgharib, Gaurav Bharaj, Florian Bernard, Hans-Peter Seidel, Patrick Perez, Michael Zollhofer, and Christian Theobalt. StyleRig: Rigging StyleGAN for 3D Control Over Portrait Images. In *Proceedings of the IEEE/CVF Conference on Computer Vision and Pattern Recognition (CVPR)*, June 2020. 2

[45] Ting-Chun Wang, Ming-Yu Liu, Jun-Yan Zhu, Andrew Tao, Jan Kautz, and Bryan Catanzaro. High-Resolution Image Synthesis and Semantic Manipulation with Conditional GANs. In *Proceedings of the IEEE Conference on Computer Vision and Pattern Recognition CVPR*, 2018. 2

[46] Ceyuan Yang, Yujun Shen, and Bolei Zhou. Semantic Hierarchy Emerges in Deep Generative Representations for Scene Synthesis. *arXiv preprint arXiv:1911.09267*, 2019. 2

[47] Hengshuang Zhao, Jianping Shi, Xiaojuan Qi, Xiaogang Wang, and Jiaya Jia. Pyramid Scene Parsing Network. In *CVPR*, 2017. 4

[48] Jiapeng Zhu, Yujun Shen, Deli Zhao, and Bolei Zhou. In-domain GAN Inversion for Real Image Editing. In *Proceedings of European Conference on Computer Vision (ECCV)*, 2020. 8

[49] Jun-Yan Zhu, Taesung Park, Phillip Isola, and Alexei A Efros. Unpaired Image-to-Image Translation using Cycle-Consistent Adversarial Networks. In *IEEE International Conference on Computer Vision ICCV*, 2017. 2